CrossMark

CLASS: Coronal Line Activity Spectroscopic Survey

Michael Reefe[1,4] , Shobita Satyapal[1] , Remington O. Sexton[1,2] , Sara M. Doan[1] , Nathan J. Secrest[2] , and Jenna M. Cann[3,5]
[1] George Mason University, Department of Physics and Astronomy, MS3F3, 4400 University Drive, Fairfax, VA 22030, USA; mreefe@gmu.edu
[2] U.S. Naval Observatory, 3450 Massachusetts Avenue NW, Washington, DC 20392-5420, USA
[3] NASA Goddard Space Flight Center, 8800 Greenbelt Rd, Greenbelt, Maryland 20771 USA

Abstract

We conduct the first systematic survey of a comprehensive set of the twenty optical coronal lines in the spectra of nearly 1 million galaxies observed by the Sloan Digital Sky Survey (SDSS) Data Release 8 catalog. This includes often overlooked high ionization potential lines such as [Ar X] $\lambda5533$, [S XII] $\lambda7609$, [Fe XI] $\lambda7892$, and [Fe XIV] $\lambda5303$. We find that, given the limited sensitivity of SDSS, strong coronal line emission is extremely rare, with only $\sim0.03\%$ of the sample showing at least one coronal line, significantly lower than the fraction of galaxies showing optical narrow line ratios ($\sim17\%$) or mid-infrared colors ($\sim2\%$) indicative of nuclear activity. The coronal line luminosities exhibit a large dynamic range, with values ranging from $\sim10^{34}$ to 10^{42} erg s^{-1}. We find that a vast majority ($\sim80\%$) of coronal line emitters in dwarf galaxies ($M_* < 9.6 \times 10^9\ M_\odot$) do not display optical narrow line ratios indicative of nuclear activity, in contrast to higher mass galaxies ($\sim17\%$). Moreover, we find that the highest ionization potential lines are preferentially found in lower mass galaxies. These findings are consistent with the theory that lower mass black holes found in lower mass galaxies produce a hotter accretion disk, which in turn enhances the higher ionization coronal line spectrum. Future coronal line searches with 30 m class telescopes or JWST may provide a pathway into uncovering the intermediate mass black hole population.

Unified Astronomy Thesaurus concepts: Active galaxies (17); Starburst galaxies (1570); Galaxy evolution (594); Dwarf galaxies (416); Infrared galaxies (790); Interstellar medium (847); Emission line galaxies (459); Galaxy accretion disks (562)

1. Introduction

High ionization fine-structure lines have been known to exist in the optical spectra of nearby active galactic nuclei (AGNs) for almost sixty years (e.g., Oke & Sargent 1968; Nussbaumer & Osterbrock 1970; Grandi 1978; Penston & Perez 1984; Appenzeller & Oestreicher 1988; Prieto et al. 2002; Lamperti et al. 2017; Müller-Sánchez et al. 2018). These so-called "coronal lines", first observed in the solar corona, arise from collisionally excited forbidden fine-structure transitions in highly ionized species, with ionization potentials that extend well beyond the Lyman limit to several hundred electron volts. This corresponds to the so-called "Big Blue Bump" thought to arise from accretion disk emission (e.g., Lynden-Bell 1969; Mushotzky & Ferland 1984; Netzer 1985; Pogge & Peterson 1992) and the "soft excess" characteristic of AGN soft X-ray spectra (Krolik 1999; Boissay et al. 2016). While systematic surveys of the strong emission lines seen in the optical spectra of galaxies have now been carried out on millions of galaxies, and their diagnostic potential in studying star formation and accretion activity are well established (e.g., Kauffmann et al. 2003; Brinchmann et al. 2004), no such large scale systematic survey of the much weaker coronal lines has been carried out on similarly large samples of galaxies. Because of their high ionization potentials and high critical

densities ($\sim10^7$–10^{10} cm^{-3}), coronal lines are powerful probes of the highly ionized and dense gas in galaxy centers. They have the potential to identify elusive AGNs missed by optical narrow line ratios and mid-infrared color selection which suffer from contamination from star formation in the host galaxy (e.g., Goulding & Alexander 2009; Trump et al. 2015; Satyapal et al. 2018, 2021), and may actually be a powerful tool in identifying accreting intermediate mass black holes (IMBHs) (e.g., Cann et al. 2018; Molina et al. 2021a, 2021b; Cann et al. 2021).

Coronal lines can indirectly probe the spectral energy distribution (SED) of the ionizing radiation field from the Lyman limit up to several hundred electron volts, a region of the electromagnetic spectrum that is observationally inaccessible because of Galactic and intrinsic absorption (e.g., Moorwood et al. 1996; Alexander et al. 2000). As a result, they can potentially be used to constrain accretion disk models, and even possibly the mass of the black hole (Cann et al. 2018; Prieto et al. 2022). The resulting intrinsic SED is also of interest in studying the effect of the AGN on its environment, and the line ratios can also be used to infer the gas density and temperature of the highly ionized and dense gas close to the central supermassive black hole (SMBH). Finally, because the line profiles often show asymmetrical profiles indicative of outflows, with outflow properties often showing correlations between ionization potential and critical density (e.g., Erkens et al. 1997; Rodríguez-Ardila et al. 2006; Bohn et al. 2021), coronal lines can be used to study outflows in the most highly ionized gas near their launch origin, a crucial input in understanding AGN feedback and its impact on star formation in the host galaxy.

With the advent of the next generation of 30 m class extremely large telescopes (ELTs), unprecedented sensitivity and spatial resolution will become possible within the coming decade. Large scale surveys of the fainter coronal lines will be feasible, resulting in transformative advances in our understanding of the highly ionized gas in galaxy centers with extremely high spatial resolution. While most past optical and near-infrared coronal line studies have exclusively targeted AGNs (Rodríguez-Ardila et al. 2002; Riffel et al. 2006; Müller-Sánchez et al. 2011; Rodríguez-Ardila et al. 2011; Lamperti et al. 2017; Müller-Sánchez et al. 2018), there have been a few studies aimed at the general galaxy population. In a large scale search for [Fe X] $\lambda6374$ emission, Gelbord et al. (2009) identified 63 galaxies with detections, all of which were previously identified as AGNs. Recently, Negus et al. (2021) conducted an extensive search for coronal line emission in integral field data and found 10 coronal line emitters, seven of which were known AGNs, all showing spatially extended emission. In other recent work, Molina et al. (2021b) searched for [Fe X] $\lambda6374$ emission in a large sample of dwarf galaxies, finding convincing evidence for previously hidden AGNs in the dwarf galaxy population. These studies have hinted at the diagnostic potential of coronal lines in the general galaxy population and have provided tantalizing evidence for their power in uncovering previously unidentified AGNs, but no study thus far has explored all of the optically accessible coronal lines in any sample, and studies of a comprehensive set of optical coronal lines in large samples of galaxies do not yet exist. The full diagnostic potential of coronal lines from current optical surveys has therefore not yet been extracted.

In this work, we introduce the Coronal Line Activity Spectroscopic Survey (CLASS) for the Sloan Digital Sky Survey (SDSS) catalog. We quantify for the first time the detection statistics for all optical coronal lines detected in the SDSS spectra of a large sample of galaxies, and analyse the host galaxy demographics of coronal line emitters compared to those from other galaxy classes, and the sample as a whole. The full CLASS catalog, with an in-depth description of our methodology and all coronal line fluxes and kinematics, is presented in M. Reefe et al. (2022b, in preparation). Throughout this paper, we assume a flat ΛCDM cosmology with $H_0 = 70$ km s^{-1} Mpc^{-1}, $\Omega_m = 0.3$, and $\Omega_\Lambda = 0.7$.

2. Sample Selection and Methodology

The creation of the CLASS catalog begins with the SDSS MPA/JHU DR8 catalog (Gunn et al. 2006; Eisenstein et al. 2011; Aihara et al. 2011; Smee et al. 2013),[6] which contains 952,138 optical ($\sim$3300–8000 Å) spectra of galaxies. We choose this data release in particular to utilize the derived host galaxy properties available for each spectrum, including stellar masses and star formation rates. We perform no initial preselection on this sample based on nuclear activity and instead conduct a search for all coronal line emission in the entire extragalactic population. In this work, we systematically search for every coronal line that is present at optical wavelengths, from the [Ne V] $\lambda\lambda3346,3426$ doublet at the blue end to the high ionization potential [Fe XI] $\lambda7892$ at the red end. We note that most previous coronal line searches have exclusively targeted already identified AGNs, or are based on a single or small set of coronal lines. Moreover, previous studies

often impose requirements on the detection or widths of other lines (e.g., [O I] $\lambda6302$ for [Fe X] $\lambda6374$ searches) and use these as preselection strategies in generating the final sample. We emphasize that our methodology is designed to be inclusive, with no bias imposed in our preselection strategy. Our goal is to gain an understanding of the demographics of coronal line activity in the general galaxy population and to quantify for the first time their detection rates. The full list of coronal lines can be found in Table 1.

We construct a sample of candidate coronal line emitters by applying a preselection filtering algorithm to search for robust detections. For each of the coronal lines listed in Table 1, we perform a linear fit to the continuum using two adjacent reference regions ±30 Å on either side of the the line of interest, adjusting the location as necessary to ensure that they fall on a flat and featureless part of the continuum, and subtract this from the average flux in a 20 Å region centered on the coronal line. We then calculate the rms deviation of the flux in the adjacent reference windows, which quantifies the noise in the continuum, and requires that the average flux centered on each coronal line is at least 4σ above the noise. This filtering is achieved with a custom-made Python package called BIFRÖST.[7] We note that this preselection algorithm is designed to identify the most robust detections in the entire sample, and will necessarily exclude marginal detections.

To eliminate spurious detections and contamination from nearby sky lines, we impose the additional constraints that our coronal line candidate spectra must have at least three continuous pixels above 3σ and must not be within ±20 Å (or $\sim\pm1000$ km s^{-1}) of the four most prominent sky lines at 5578.5, 5894.6, 6301.7, and 7246.0 Å, respectively.

The resulting sample of 2834 candidate spectra were then fit using the Bayesian AGN Decomposition Analysis for SDSS Spectra (BADASS; Sexton et al. 2020) software. Spectra are fit with BADASS first using a likelihood maximization routine from SciPy, followed by a Markov Chain Monte Carlo (MCMC) fit using the affine-invariant Emcee sampler (Foreman-Mackey et al. 2013) to obtain robust uncertainties and covariances. The BADASS fitting routine breaks down a spectrum into its base components, modeling the AGN power-law continuum, Fe II emission, and spectral lines simultaneously with the stellar line-of-sight velocity distribution (LOSVD) using the penalized pixel-fitting (pPXF; Cappellari 2017) method. Each coronal line is modeled as a simple Gaussian profile with a free amplitude, velocity offset, and width. We also do not fit the entire wavelength range of the spectrum at once, but instead subdivide it into smaller regions of a few hundred ångströms to glean basic information about the continuum level. We require the model-fit flux of each line to be above 3σ.

For a few specific lines, we impose additional constraints on certain parameters. Doublets such as [Fe VII] $\lambda\lambda5720,6087$ have their widths and offsets tied. The flux ratio of the [O I] $\lambda\lambda6302,6365$ doublet is fixed to 3, as predicted by atomic physics, and the line widths and velocity offsets are both tied to [N II] $\lambda6585$, ensuring that the nearby [Fe X] $\lambda6374$ can be robustly distinguished from [O I].

We then perform a final round of visual inspection before confirming each coronal line detection. We present a selection of six individual spectra that show some of the most commonly

Table 1
Optical Coronal Emission Lines from 3346 to 7892 Å

Line	Wavelength[a] (Å)	Critical Density (cm^{-3})	Ionization Potential[b] (eV)	Transition	Luminosity $\log L/$ erg s^{-1} (dex)	Detections (%)	Number
[Fe XI]	7891.800	6.39×10^{8}	262.10	$^{3}P_{2} - {}^{3}P_{1}$	38.92 ± 1.27	$0.0064^{+0.0029}_{-0.0021}$	9/141510
[S XII]	7611.000	7.09×10^{9}	504.78	$^{2}P^{0}_{1/2} - {}^{2}P^{0}_{3/2}$	39.40 ± 0.28	$0.00058^{+0.00076}_{-0.00037}$	2/344071
[Fe X]	6374.510	4.45×10^{8}	235.04	$^{2}P^{0}_{3/2} - {}^{2}P^{0}_{1/2}$	39.00 ± 1.05	$0.0407^{+0.0043}_{-0.0039}$	107/262586
[Fe VII]	6087.000	4.46×10^{7}	99.00	$^{3}F_{3} - {}^{1}D_{2}$	39.96 ± 0.59	$0.0146^{+0.0015}_{-0.0014}$	111/758853
[Fe VII]	5720.700	3.72×10^{7}	99.00	$^{3}F_{2} - {}^{1}D_{2}$	39.77 ± 0.59	$0.0158^{+0.0016}_{-0.0015}$	114/722973
[Ar X]	5533.265	2.36×10^{9}	422.60	$^{2}P^{0}_{3/2} - {}^{2}P^{0}_{1/2}$	38.83 ± 2.83	$0.0028^{+0.0019}_{-0.0012}$	5/181285
[Fe VI]	5335.180	6.32×10^{6}	75.00	$^{4}F_{3/2} - {}^{4}P_{1/2}$	39.74 ± 2.14	$0.00131^{+0.00064}_{-0.00045}$	8/612802
[Ca V]	5309.110	6.63×10^{7}	67.10	$^{3}P_{2} - {}^{1}D_{2}$	40.11 ± 0.58	$0.00137^{+0.00055}_{-0.00040}$	11/805788
[Fe XIV]	5302.860	3.99×10^{8}	361.00	$^{2}P^{0}_{1/2} - {}^{2}P^{0}_{3/2}$	39.94 ± 0.66	$0.00095^{+0.00051}_{-0.00035}$	7/733674
[Fe VII]	5276.380	2.98×10^{6}	99.00	$^{3}F_{4} - {}^{3}P_{2}$	37.08 ± 1.76	$0.0057^{+0.0026}_{-0.0018}$	9/158631
[Fe VI]	5176.040	3.29×10^{7}	75.00	$^{4}F_{9/2} - {}^{2}G_{9/2}$	39.47 ± 2.55	$0.00070^{+0.00068}_{-0.00038}$	3/429814
[Fe VII]	5158.890	3.44×10^{6}	99.00	$^{3}F_{3} - {}^{3}P_{1}$	37.70 ± 1.45	$0.0025^{+0.0020}_{-0.0012}$	4/161259
[Fe VI]	5145.750	2.29×10^{7}	75.00	$^{4}F_{7/2} - {}^{2}G_{7/2}$	40.65 ± 0.48	$0.00077^{+0.00041}_{-0.00028}$	7/904885
[Fe VII]	4893.370	3.09×10^{6}	99.00	$^{3}F_{2} - {}^{3}P_{1}$	38.94 ± 2.21	$0.0054^{+0.0036}_{-0.0023}$	5/92997
[Fe V]	4180.600	1.86×10^{8}	54.80	$^{5}D_{1} - {}^{3}P2_{0}$	39.45 ± 2.15	$0.00117^{+0.00079}_{-0.00051}$	5/425954
[Fe V]	3891.280	1.61×10^{8}	54.80	$^{5}D_{4} - {}^{3}F2_{4}$	40.62 ± 1.06	$0.00022^{+0.00029}_{-0.00014}$	2/905489
[Fe V]	3839.270	1.00×10^{8}	54.80	$^{5}D_{3} - {}^{3}F2_{3}$	41.20 ± 0.60	$0.00054^{+0.00037}_{-0.00023}$	5/919435
[Fe VII]	3758.920	4.02×10^{7}	99.00	$^{3}F_{4} - {}^{1}G_{4}$	40.38 ± 0.90	$0.00097^{+0.00048}_{-0.00033}$	8/823110
[Ne V]	3425.881	1.90×10^{7}	97.11	$^{3}P_{2} - {}^{1}D_{2}$	41.21 ± 0.29	$0.0123^{+0.0018}_{-0.0016}$	61/497710
[Ne V]	3345.821	1.14×10^{7}	97.11	$^{3}P_{1} - {}^{1}D_{2}$	40.91 ± 0.24	$0.0085^{+0.0018}_{-0.0015}$	31/365647

Notes. For the luminosity, the values shown are (mean) $\pm$ (standard deviation). The detection confidence levels are 68%.
[a] Wavelengths taken from: https://physics.nist.gov/PhysRefData/ASD/lines_form.html.
[b] Ionization potential taken from: https://physics.nist.gov/PhysRefData/ASD/ionEnergy.html.

detected coronal lines in Figure 1, with the spectral fit overlaid. Our final sample contains 258 galaxies (∼0.03% of the catalog). The coronal line luminosities in our sample range from 10^{34}–10^{42} erg s^{-1}, with a median value of 1.08×10^{40} erg s^{-1}. The average and standard deviation of the luminosity for each coronal line is listed in Table 1. The redshifts of our coronal line sample ranged from 0 to 0.3, with an average of 0.105 ± 0.100.

The galaxies in our sample are classified as AGNs or star-forming (SF) galaxies based on optical narrow emission line ratios, using the Baldwin–Phillips–Terlevich (BPT) diagnostics (Baldwin et al. 1981), as well as mid-infrared color selection. For optical selection, we use the K03 (Kauffmann et al. 2003) and K01 (Kewley et al. 2001) selection criteria to classify spectra as AGNs or SF galaxies using the fluxes provided in the MPA/JHU catalog, requiring a signal-to-noise ratio >3 on the relevant narrow line detections. In order to classify galaxies in the sample according to their mid-infrared color, we matched the MPA/JHU DR8 catalog to the final public AllWISE catalog,[8] where a galaxy is matched if the positions agree to within 6″. We require that all objects be detected with a signal-to-noise ratio >5 in the 3.4 μm W1 and 4.6 μm W2 bands in order to employ a mid-infrared color diagnostic. We use the three-band AGN color cut from Jarrett et al. (2011) to identify mid-infrared AGNs in the sample. In order to obtain information on the host galaxy morphologies, we use the magnitudes and Sérsic indices, obtained from single comp-onent two-dimensional fits to the surface brightness profiles, from the NASA–Sloan Atlas (NSA) catalog (version 1.0.1).[9]

One of our goals is to quantify the detection statistics for each of the 20 coronal lines in this study. Because the luminosities of the various coronal lines vary considerably, as do the signal-to-noise ratios of the observations, the total number of spectra employed in the calculated detection fraction varies from line to line. In particular, in calculating the detection fractions, we exclude from consideration spectra in which the sensitivity is not sufficient to enable a 3σ detection of the given coronal line with a luminosity equal to the average luminosity among our detections. In addition, in calculating each detection fraction, we exclude from consideration spectra in which the given coronal line is redshifted out of the SDSS spectral range. We calculate the sensitivity of each spectrum by integrating a Gaussian with an amplitude equal to the rms of the flux and width equal to the instrumental FWHM dispersion, both calculated at the location of the coronal line. This allows us to account for the nonuniform sensitivity of the observations to each of the coronal lines, allowing their detection percentages to be directly comparable to each other, given the sensitivity of SDSS.

3. Results

3.1. Detection Statistics and Comparison with Other Diagnostics

We find that coronal line emission is extremely rare in the SDSS spectra of galaxies. Given the total sample of 258 galaxies that display at least one coronal line identified through our pipeline, the detection fraction using binomial statistics, with 68% confidence bounds, is $0.0271^{+0.0018}_{-0.0017}$%, significantly lower than the fraction obtained using other commonly employed diagnostics for nuclear activity. In comparison, the

[8] https://wise2.ipac.caltech.edu/docs/release/allwise/
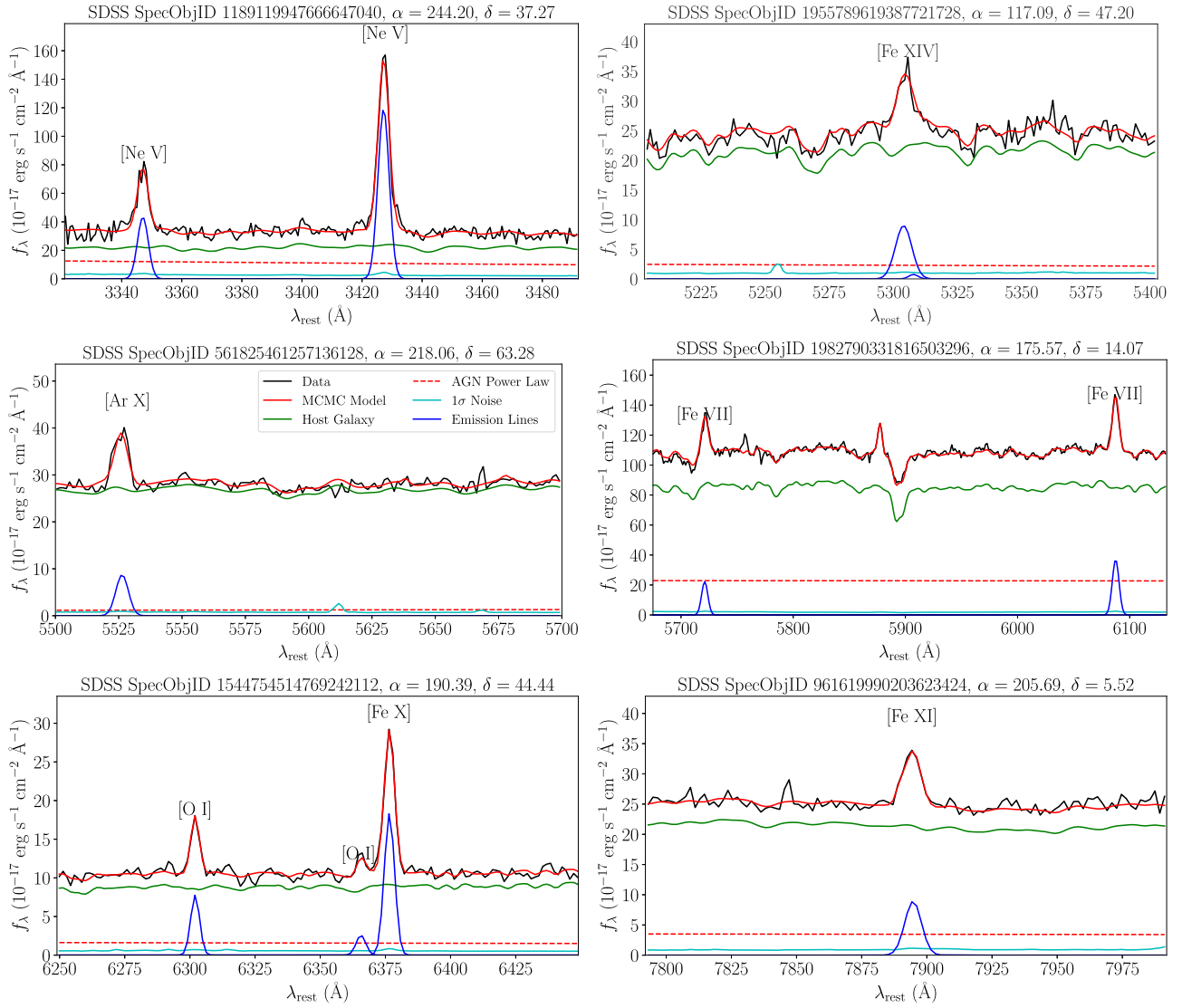[9] https://www.sdss.org/dr13/manga/manga-target-selection/nsa/

Figure 1. Examples of six individual spectra that exhibit emission of at least one coronal line in the optical. The SDSS data, corrected for redshift and galactic extinction, are plotted in black, while the model and each of its components (AGN power law, host galaxy, and emission lines) are overlaid on the spectra. Each coronal line is labeled, along with the (non-coronal) [O I] line in the [Fe X] spectrum, and the object's SDSS Spec Object ID and coordinates are labeled in each plot's title.

detection fraction of galaxies identified as K01 AGNs and WISE AGNs is $16.821\% \pm 0.031\%$ and $2.002^{+0.012}_{-0.011}\%$, respectively. The detection fraction and luminosity distributions vary considerably for the various lines, as can be seen from Table 1. Among the most commonly found coronal lines are [Fe X] $\lambda 6374$, the [Fe VII] $\lambda\lambda 6087,5720$ doublet, and the [Ne V] $\lambda\lambda 3346,3426$ doublet, with detection fractions upwards of 0.0407%. The least common, on the other hand, are [S XII] $\lambda 7609$, and [Fe V] $\lambda 3891$ with only two detections. The maximum number of coronal lines that we detect together in a single galaxy is only six, with two such galaxies, SDSS specObjIDs 2411797517822879744 and 2904951020922628096. The former exhibits [Fe XI] $\lambda 7892$, [Fe X] $\lambda 6374$, [Fe VII] $\lambda\lambda 6087,5720$, [Ca V] $\lambda 5309$, and [Fe VII] $\lambda 5159$. The latter exhibits almost the same set of lines, but shows [Fe XIV] $\lambda 5303$ instead of [Fe VII] $\lambda 5159$. It is clear from this study that it is rare to detect many coronal lines in a single spectrum; 49% of the coronal line emitting galaxies have only one coronal line detected. We note that because our filtering algorithm is designed to pick out robust detections and

therefore may exclude marginal detections, our catalog does not include all coronal line detections reported previously in the literature (e.g., Gelbord et al. 2009; Molina et al. 2021b). We examine the overlap between the various samples in more detail in M. Reefe et al. (2022b, in preparation).

The most luminous coronal line detected in the sample is [Ne V] $\lambda 3426$, with an average luminosity of 1.62×10^{41} erg s^{-1}. The strength of this line, in conjunction with its low ionization potential and its location in a relatively flat part of the spectrum is consistent with the [Ne V] $\lambda\lambda 3426,3346$ doublet having one of the highest detection fractions seen in the optical. The next most luminous line is the [Fe V] $\lambda 3839$, with an average luminosity of 1.58×10^{41} erg s^{-1}. We note that the [Fe V] doublet is located nearly directly on top of two higher-order Balmer lines, Hζ at 3889 Å and Hη at 3835 Å, making the detection of the line more challenging. Within the few detections for [Fe V] that we claim, the lower-order Hε is not visible in the spectra, so it is unlikely our results are contaminated by these Balmer lines. The least luminous coronal line in the sample is [Fe VII] $\lambda 5276$, with an average
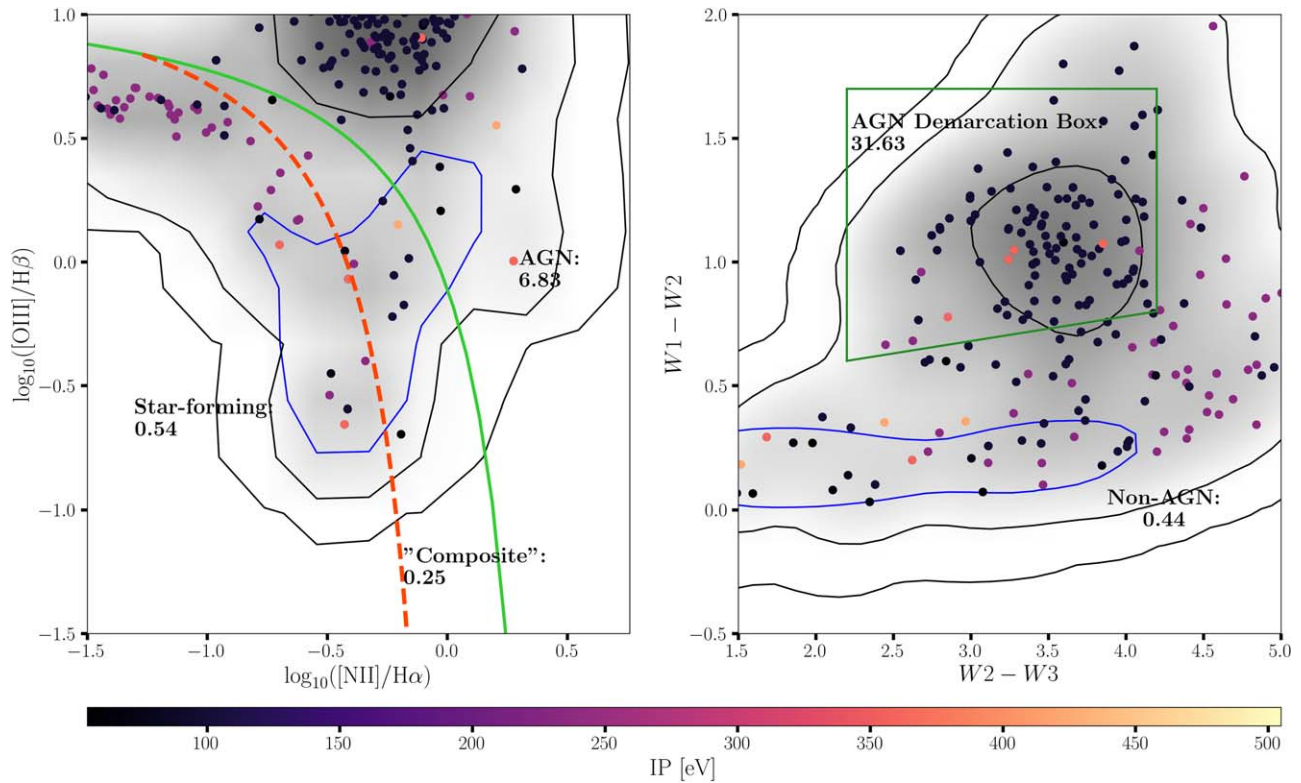
Figure 2. Left: a BPT ratio plot of all the galaxies in our subsample that have BPT information. The color of each point corresponds to the ionization potential of the most energetic coronal line detection in the galaxy. The SF, "composite," and AGN regions are marked with text and separated by the curves defined by Kauffmann et al. (2003) and Kewley et al. (2001). The black contours and shading highlight the probability density of the subsample, while the blue contour shows the 68% threshold of the entire MPA/JHU DR8 catalog. Each region is also annotated under its label with the excess of coronal line detections in that region, defined as the fraction of coronal line detections over the total number of spectra in that region, normalized by the overall coronal line detection fraction (0.0271%). Right: a WISE color–color plot of all the galaxies in our subsample that have WISE observations. The coloring of the points and contours is defined the same way as the BPT plot. The AGN demarcation box is defined from Jarrett et al. (2011).

luminosity of 1.20×10^{37} erg s^{-1}, potentially making it the most difficult line to detect in the optical.

In Figure 2, we show the narrow line ratios employed in the BPT diagram (Baldwin et al. 1981) and WISE (Wright et al. 2010) colors of our coronal line sample in comparison to the entire catalog, together with the standard AGN demarcation lines employed in the literature. The highest ionization potential of the coronal lines detected in a galaxy is indicated by the color bar. While a large fraction of our coronal line emitters do reside in the K01 region (72%), and mid-infrared AGN region (59%), a significant fraction of the coronal line emitters (11%) are not identified as AGNs using optical narrow line ratios or mid-infrared color selection. Moreover, a key and striking result of this work is that the majority of the [Fe X] and higher ionization potential detections are found in the SF region of the BPT plot and outside the Jarrett AGN box in the WISE plot. Note that although AGNs are expected to produce a hard radiation field, coronal line emission is not universally seen in either BPT-selected or mid-infrared selected AGNs, a result that is consistent with numerous other studies (e.g., Nagao et al. 2000; Riffel et al. 2006; Lamperti et al. 2017). Only ~0.2% and ~0.9% of BPT and mid-infrared AGNs showed coronal line emission detectable by SDSS in our sample. Given the average luminosity of the coronal lines that are detected in our sample, and considering only those observations with the sensitivity to detect them, only 0.2% of K01 and 6.1% of WISE AGNs display coronal line emission identified in our pipeline. Luminous optical coronal line emission is therefore

intrinsically rare, a result that is explored by J. McKaig et al. (2022, in preparation).

3.2. Host Galaxy Properties

Having identified coronal line emitters in SDSS, we now explore the host galaxy demographics of this population and compare them to those of other galaxy subclasses. Specifically, we explore the SFRs, stellar masses, and galaxy morphologies of the sample. We use the the [N II]/Hα ratio, the most robust metallicity indicator in galaxies where the primary source of ionization is not well-constrained (e.g., Groves et al. 2006) to gain insight into the metallicity of the host galaxies of our sample in comparison to other subclasses. In comparing host galaxy morphology, we use the Sérsic index, n_{sersic}, with low values indicating disk-like morphologies and higher values corresponding to bulge-dominated morphologies. Because the Sérsic fits depend on the spatial extent and hence distance to the galaxies, we match by r-band magnitude when comparing Sérsic indices in BPT-AGNs with coronal line emitters. In Figure 3, we plot the SFR against the stellar mass of our sample with the main sequence relationship from McGaugh et al. (2017) overlaid. The highest ionization potential coronal line detected in a given galaxy is indicated by the color bar. As can be seen, a significant fraction of the coronal line detections (50 galaxies, or 19.4% of the 258 coronal line emitters) lies more than 1σ away from the main sequence relationship, with the vast majority of the higher ionization potential coronal line detections preferentially found well above the relationship.
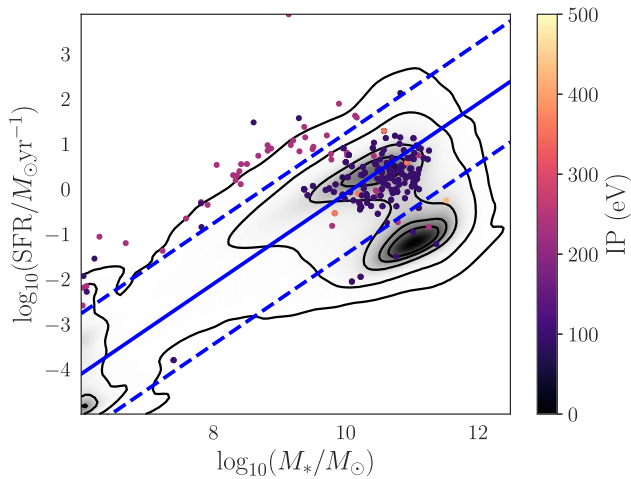
Figure 3. Galaxy star formation rate vs. stellar mass. A Gaussian kernel density estimation of the full MPA/JHU catalog is plotted in gray, while our coronal line detections are plotted individually, colored by the ionization potential. The main sequence relationship from McGaugh et al. (2017) is plotted in blue, and the 1σ standard deviation of the full sample is shown in the dashed blue lines.

Similar results are found by Molina et al. (2021b) in their sample of [Fe X]-emitting dwarf galaxies. While it is clear that coronal line emission is preferentially seen in galaxies with elevated SFRs, this does not necessarily imply that the emission lines are generated by stellar processes, as pointed out by Molina et al. (2021b). Elevated accretion activity onto a SMBH or an elevated tidal disruption event (TDE) rate may be correlated with an elevated SFR in galaxies, as available nuclear gas may provide the fuel for both accretion and star formation activity. There is no correlation seen between the host galaxy specific SFR and coronal line luminosity, a result we explore further in M. Reefe et al. (2022b, in preparation)

In Figure 4, we explore the host galaxy demographics of the coronal line emitters relative to those of BPT-selected and WISE AGNs. In these plots, we only consider emission line galaxies in which the [O III] line is detected with a signal-to-noise ratio $\geqslant 5$, which constitutes $\sim 1/3$ of the original sample, and plot the fraction of galaxies in various subclasses of nuclear activity. We replicate the well-known trend that optical narrow line diagnostics select AGNs in more massive (Figure 4(a)), metal-rich (Figure 4(c)), and bulge-dominated (Figure 4(d)) hosts (see Figure 5 in Kauffmann et al. 2003). In contrast, we do not see the same dramatic drop in coronal line emitters and WISE AGNs in lower mass galaxies, despite the fact that the lower mass galaxies suffer greater flux incompleteness. Moreover, a key and striking result from this work is that there is a dramatic increase with decreasing stellar mass in coronal line emitters that are not identified as BPT-AGNs, as can be seen by Figure 4(b). We also see in Figure 4(a) that in lower mass hosts, the higher ionization potential coronal lines are more prevalent than the lower ionization potential lines, in contrast to what is found in the higher mass galaxies. Coronal line emitters are also found in lower metallicity galaxies based on their [N II]/Hα ratios, as can be seen in Figure 4(c). Higher ionization potential coronal lines also possibly favor disk-like hosts compared with lower ionization potential lines and BPT-selected AGN hosts (Figure 4(d)). While the limited sample size of coronal line emitters precludes us from conducting a statistically rigorous analysis, this study clearly demonstrates that coronal line emission is uncovering a different host galaxy

population than is revealed by traditional optical narrow line ratios.

4. Discussion and Conclusions

We have constructed CLASS, with the goal of providing for the first time a complete census of all optical coronal line emission in the galaxy population observed by SDSS. Our survey is designed to pick out all robust detections of the 20 optical coronal lines accessible in the SDSS wavelength regime; marginal detections are not included in the current survey. We find that optical coronal line emission is extremely rare in the galaxy population, even in AGNs identified through optical narrow line ratios or mid-infrared color selection, and even when accounting for the sensitivity of SDSS. Our detection rate in AGNs is significantly lower than that seen in the near-infrared spectra of AGNs (Rodríguez-Ardila et al. 2011; Lamperti et al. 2017; Müller-Sánchez et al. 2018), possibly due to dust extinction, a result that underscores the crucial need for JWST in future coronal line studies. This study also demonstrates that, while rare, a significant fraction of coronal line emitters are found in galaxies with no signs of nuclear activity based on their optical narrow line ratios or mid-infrared color, with the majority of coronal line emitters with no optical or mid-infrared AGN indication being found in lower mass hosts. Coronal line emitters are preferentially found in galaxies with elevated star formation rates, and tend to reside in more metal-poor and later-type galaxies compared to BPT-AGNs.

In this work, we have not explored the origin of the coronal line emission, but instead our goal is to provide a complete census of coronal line activity in SDSS and explore their host galaxy properties. Optical coronal line emission has been observed in extragalactic supernovae (Benjamin & Dinerstein 1990; Smith et al. 2009; Izotov & Thuan 2009), and can be produced by Wolf-Rayet stars, planetary nebula, or shocks from starburst-driven winds (Schaerer & Stasińska 1999; Abel & Satyapal 2008; Allen et al. 2008; Zhang et al. 2012), but their luminosities are generally significantly lower than the luminosities of the coronal lines presented in this work. Photoionization from stars in lower metallicity galaxies can also potentially produce coronal lines. Lower metallicity galaxies are dominated by more massive stars which produce a harder radiation field (Campbell et al. 1986), which in turn can produce an emission line spectrum dominated by higher ionization potential lines, a result that has been observed with the detection of [Ne V] $\lambda\lambda3346,3426$ in blue compact dwarf galaxies (Izotov et al. 2012, 2021). However, we reiterate that the luminosities of the coronal lines in this sample are generally larger than those produced by purely stellar processes, ranging from 1 to 2 orders of magnitude above those typically seen from stellar processes. Finally, coronal line emission can be produced by TDEs or accretion onto a SMBH (Wang et al. 2012). If this is the case, the prevalence of coronal line emission in dwarf galaxies in our sample, with the lines with the highest ionization potential preferentially found in lower mass hosts, is consistent with the theory that lower mass hosts with lower mass black holes produce a hotter accretion disk, which in turn enhances the high ionization coronal line spectrum (Cann et al. 2018) and causes the optical narrow line ratios employed in the BPT diagram to be indistinguishable from those of SF galaxies (Cann et al. 2019). In M. Reefe et al. (2022b, in preparation), we present an in-depth
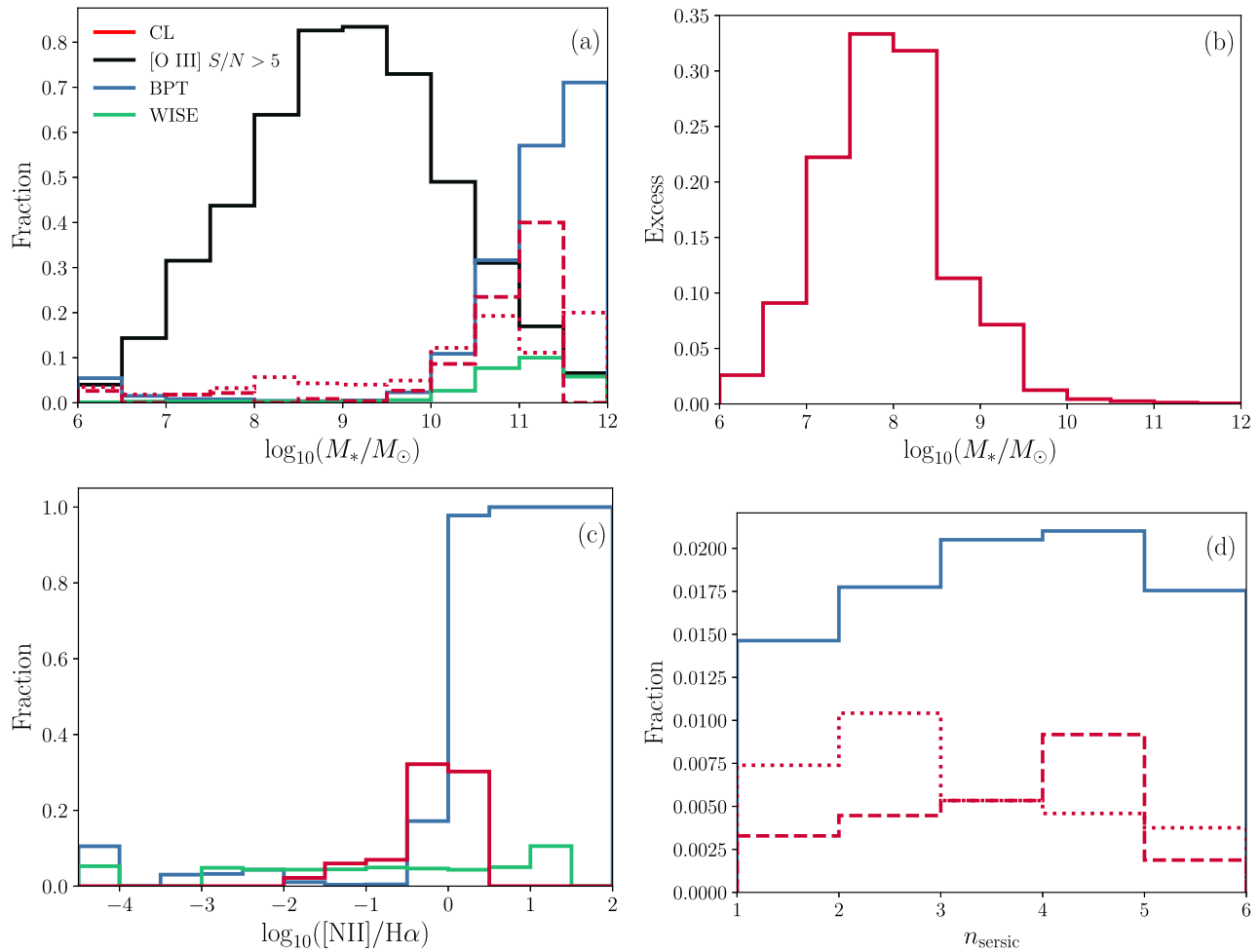
Figure 4. Histograms of various subsets of our galaxy sample, with stellar mass, metallicity, and Sérsic index on the abscissae. The ordinate is the fraction of galaxies that meet certain criteria within each bin. The solid black line is the fraction of the full galaxy sample of 952,138 that have an [O III] signal-to-noise ratio $\geqslant 5$, the solid blue line is the fraction of those galaxies that meet the [O III] signal-to-noise ratio requirement (of which there are 354,905) that are classified as AGN via their BPT ratios using the Kewley et al. (2001) criterion, and the solid green line is the fraction of the [O III] galaxies that are classified as AGNs by their WISE colors as in Jarrett et al. (2011). The red lines indicate the fraction of coronal line emitters out of the initial subsample of 2834 candidates marked by the BIFRÖST analysis which also meet the [O III] signal-to-noise ratio threshold, of which there are 1651. The solid line includes all coronal line emitters, the dashed line includes only those with ionization potentials <200 eV, and the dotted line includes only those with ionization potentials >200 eV. In panel b, we plot the excess of coronal line detections as a fraction of BPT-identified AGNs from panel a, of which there are 62,410. In panel d, the data are subsampled such that the distributions in r magnitude match between the control BPT-AGNs and the sample coronal line emitters–the BPT fraction is again out of the full sample, while the coronanl line fraction is out of the r-magnitude-matched BPT subsample, of which there are 5,100.

description of the CLASS catalog, provide the full list of line fluxes and kinematics, and explore the origin of the coronal line emission in our sample. Given the sensitivity of SDSS and the faintness of coronal line emission, more sensitive surveys are critical to unlock their full diagnostic potential. Infrared coronal lines are significantly stronger than optical coronal lines. For example, in the nearby AGN, Circinus, the infrared coronal lines are up to over two magnitudes more luminous than the optical coronal lines (Oliva et al. 1994; Moorwood et al. 1996), with an even more significant enhancement of the infrared coronal lines relative to the optical coronal lines anticipated for IMBHs (Cann et al. 2018). Follow-up observations with JWST may thus be a powerful avenue for uncovering IMBHs and constraining their properties.

---

[10] http://www.astropy.org

ORCID iDs

Michael Reefe ● https://orcid.org/0000-0003-4701-8497
Shobita Satyapal ● https://orcid.org/0000-0003-2277-2354
Remington O. Sexton ● https://orcid.org/0000-0003-3432-2094
Sara M. Doan ● https://orcid.org/0000-0003-3152-4328
Nathan J. Secrest ● https://orcid.org/0000-0002-4902-8077
Jenna M. Cann ● https://orcid.org/0000-0003-1051-6564

References

Abel, N. P., & Satyapal, S. 2008, ApJ, 678, 686
Aihara, H., Allende Prieto, C., An, D., et al. 2011, ApJS, 193, 29
Alexander, T., Lutz, D., Sturm, E., et al. 2000, ApJ, 536, 710
Allen, M. G., Groves, B. A., Dopita, M. A., Sutherland, R. S., & Kewley, L. J. 2008, ApJS, 178, 20
Appenzeller, I., & Oestreicher, R. 1988, AJ, 95, 45
Astropy Collaboration, Robitaille, T. P., Tollerud, E. J., et al. 2013, A&A, 558, A33
Baldwin, J. A., Phillips, M. M., & Terlevich, R. 1981, PASP, 93, 5
Benjamin, R. A., & Dinerstein, H. L. 1990, AJ, 100, 1588
Bohn, T., Canalizo, G., Veilleux, S., & Liu, W. 2021, ApJ, 911, 70
Boissay, R., Ricci, C., & Paltani, S. 2016, A&A, 588, A70
Brinchmann, J., Charlot, S., White, S. D. M., et al. 2004, MNRAS, 351, 1151
Campbell, A., Terlevich, R., & Melnick, J. 1986, MNRAS, 223, 811
Cann, J. M., Satyapal, S., Abel, N. P., et al. 2019, ApJL, 870, L2
Cann, J. M., Satyapal, S., Abel, N. P., et al. 2018, ApJ, 861, 142
Cann, J. M., Satyapal, S., Rothberg, B., et al. 2021, ApJL, 912, L2
Cappellari, M. 2017, MNRAS, 466, 798
Eisenstein, D. J., Weinberg, D. H., Agol, E., et al. 2011, AJ, 142, 72
Erkens, U., Appenzeller, I., & Wagner, S. 1997, A&A, 323, 707
Foreman-Mackey, D., Hogg, D. W., Lang, D., & Goodman, J. 2013, PASP, 125, 306
Gelbord, J. M., Mullaney, J. R., & Ward, M. J. 2009, MNRAS, 397, 172
Goulding, A. D., & Alexander, D. M. 2009, MNRAS, 398, 1165
Grandi, S. A. 1978, ApJ, 221, 501
Groves, B., Kewley, L., Kauffmann, G., & Heckman, T. 2006, NewAR, 50, 743
Gunn, J. E., Siegmund, W. A., Mannery, E. J., et al. 2006, AJ, 131, 2332
Harris, C. R., Millman, K. J., van der Walt, S. J., et al. 2020, Natur, 585, 357
Izotov, Y. I., & Thuan, T. X. 2009, ApJ, 707, 1560
Izotov, Y. I., Thuan, T. X., & Guseva, N. G. 2021, MNRAS, 508, 2556
Izotov, Y. I., Thuan, T. X., & Privon, G. 2012, MNRAS, 427, 1229
Jarrett, T. H., Cohen, M., Masci, F., et al. 2011, ApJ, 735, 112
Kauffmann, G., Heckman, T. M., Tremonti, C., et al. 2003, MNRAS, 346, 1055
Kewley, L. J., Dopita, M. A., Sutherland, R. S., Heisler, C. A., & Trevena, J. 2001, ApJ, 556, 121
Krolik, J. H. 1999, Active galactic nuclei: from the central black hole to the galactic environment (Princeton, NJ: Princeton Univ. Press)
Lamperti, I., Koss, M., Trakhtenbrot, B., et al. 2017, MNRAS, 467, 540
Lynden-Bell, D. 1969, Natur, 223, 690
McGaugh, S. S., Schombert, J. M., & Lelli, F. 2017, ApJ, 851, 22
Molina, M., Reines, A. E., Greene, J. E., Darling, J., & Condon, J. J. 2021a, ApJ, 910, 5
Molina, M., Reines, A. E., Latimer, C. J., Baldassare, V., & Salehirad, S. 2021b, ApJ, 922, 155
Moorwood, A. F. M., Lutz, D., Oliva, E., et al. 1996, A&A, 315, L109
Müller-Sánchez, F., Hicks, E. K. S., Malkan, M., et al. 2018, ApJ, 858, 48
Müller-Sánchez, F., Prieto, M. A., Hicks, E. K. S., et al. 2011, ApJ, 739, 69
Mushotzky, R., & Ferland, G. J. 1984, ApJ, 278, 558
Nagao, T., Taniguchi, Y., & Murayama, T. 2000, AJ, 119, 2605
Negus, J., Comerford, J. M., Müller Sánchez, F., et al. 2021, ApJ, 920, 62
Netzer, H. 1985, MNRAS, 216, 63
Nussbaumer, H., & Osterbrock, D. E. 1970, ApJ, 161, 811
Oke, J. B., & Sargent, W. L. W. 1968, ApJ, 151, 807
Oliva, E., Salvati, M., Moorwood, A. F. M., & Marconi, A. 1994, A&A, 288, 457
Penston, M. V., & Perez, E. 1984, MNRAS, 211, 33P
Pogge, R. W., & Peterson, B. M. 1992, AJ, 103, 1084
Prieto, A., Rodríguez-Ardila, A., Panda, S., & Marinello, M. 2022, MNRAS, 510, 1010
Prieto, M. A., Pérez García, A. M., & Rodríguez Espinosa, J. M. 2002, MNRAS, 329, 309
Riffel, R., Rodríguez-Ardila, A., & Pastoriza, M. G. 2006, A&A, 457, 61
Rodríguez-Ardila, A., Prieto, M. A., Portilla, J. G., & Tejeiro, J. M. 2011, ApJ, 743, 100
Rodríguez-Ardila, A., Prieto, M. A., Viegas, S., & Gruenwald, R. 2006, ApJ, 653, 1098
Rodríguez-Ardila, A., Viegas, S. M., Pastoriza, M. G., & Prato, L. 2002, ApJ, 579, 214
Satyapal, S., Abel, N. P., & Secrest, N. J. 2018, ApJ, 858, 38
Satyapal, S., Kamal, L., Cann, J. M., Secrest, N. J., & Abel, N. P. 2021, ApJ, 906, 35
Schaerer, D., & Stasińska, G. 1999, A&A, 345, L17
Sexton, R. O., Matzko, W., Darden, N., Canalizo, G., & Gorjian, V. 2020, MNRAS, 500, 2871
Smee, S. A., Gunn, J. E., Uomoto, A., et al. 2013, AJ, 146, 32
Smith, N., Silverman, J. M., Chornock, R., et al. 2009, ApJ, 695, 1334
Taylor, M. B. 2005, in ASP Conf. Ser., 347, Astronomical Data Analysis Software and Systems XIV, ed. P. Shopbell, M. Britton, & R. Ebert (San Francisco, CA: ASP), 29
Trump, J. R., Sun, M., Zeimann, G. R., et al. 2015, ApJ, 811, 26
Virtanen, P., Gommers, R., Oliphant, T. E., et al. 2020, NatMe, 17, 261
Wang, T.-G., Zhou, H.-Y., Komossa, S., et al. 2012, ApJ, 749, 115
Wright, E. L., Eisenhardt, P. R. M., Mainzer, A. K., et al. 2010, AJ, 140, 1868
Zhang, Y., Fang, X., Chau, W., et al. 2012, ApJ, 754, 28